



RESEARCH LETTER

10.1002/2017GL074233

Key Points:

- Despite surface and volume dependence of cloud aqSOA and sulfate formation, their formation can be described with single drop size class
- The effective cloud droplet diameter can be used to represent cloud aqSOA and sulfate mass formation in a full size drop distribution
- A computationally efficient microphysical parameterization for in-cloud mass formation is developed for use in large-scale models

Supporting Information:

- Supporting Information S1

Correspondence to:

R. McVay,
barbara.ervens@noaa.gov

Citation:

McVay, R., and B. Ervens (2017), A microphysical parameterization of aqSOA and sulfate formation in clouds, *Geophys. Res. Lett.*, 44, 7500–7509, doi:10.1002/2017GL074233.

Received 19 MAY 2017

Accepted 5 JUL 2017

Accepted article online 18 JUL 2017

Published online 27 JUL 2017

A microphysical parameterization of aqSOA and sulfate formation in clouds

Renee McVay^{1,2,3}  and Barbara Ervens^{1,2} 

¹Cooperative Institute for Research in Environmental Sciences, University of Colorado Boulder, Boulder, Colorado, USA, ²Chemical Sciences Division, NOAA Earth System Research Laboratory, Boulder, Colorado, USA, ³Now at Environmental Defense Fund, Boulder, Colorado, USA

Abstract Sulfate and secondary organic aerosol (cloud aqSOA) can be chemically formed in cloud water. Model implementation of these processes represents a computational burden due to the large number of microphysical and chemical parameters. Chemical mechanisms have been condensed by reducing the number of chemical parameters. Here an alternative is presented to reduce the number of microphysical parameters (number of cloud droplet size classes). In-cloud mass formation is surface and volume dependent due to surface-limited oxidant uptake and/or size-dependent pH. Box and parcel model simulations show that using the effective cloud droplet diameter (proportional to total volume-to-surface ratio) reproduces sulfate and aqSOA formation rates within $\leq 30\%$ as compared to full droplet distributions; other single diameters lead to much greater deviations. This single-class approach reduces computing time significantly and can be included in models when total liquid water content and effective diameter are available.

Plain Language Summary Chemical processes in cloud water modify chemical composition and size of airborne particles that scatter or absorb light and, thus, contribute to cooling or warming of our atmosphere. Describing clouds in global models is challenging since cloud properties are often not well constrained, and clouds are smaller than model grid boxes used to numerically describe atmospheric processes. The description of chemistry in clouds is a particular computational challenge since many, both chemical (concentrations of chemical species) and microphysical (e.g., cloud droplet sizes), parameters have to be considered. While previous studies attempted to solve this problem by reducing the number of chemical parameters by combining/omitting chemical processes and/or species, we take another route by reducing the number of microphysical parameters: Previous studies suggested cloud droplet size being important to predict in-cloud formation of inorganic (sulfate) and organic particle mass. However, details on drop sizes are usually not available from measurements or models. We find that the single “effective cloud droplet diameter,” proportional to the total volume-to-surface area ratio of cloud droplets, reproduces in-cloud aerosol formation as compared to a full drop size distribution. This microphysical parameterization reduces computation time by a factor of ~ 20 and is suitable to improve prediction of chemical in-cloud mass formation in large-scale models.

1. Introduction

Clouds, and in particular aerosol-cloud interactions, contribute to large uncertainties in current understanding of radiative forcing [Intergovernmental Panel on Climate Change, 2013]. Aerosol particles can serve as cloud condensation nuclei and affect the properties of clouds; for example, an increase in aerosol particle concentration often results in more reflective clouds, enhancing their albedo [Twomey, 1977]. Clouds also affect aerosol properties and burden through in-cloud chemical and microphysical processing, vertical redistribution, and wet scavenging [Ervens, 2015]. In particular, formation of sulfate and aqueous secondary organic aerosol (aqSOA) affects aerosol loading. Both sulfate and aqSOA remain in particles upon water evaporation, modifying the physical and chemical properties of the aerosol particles, which may lead to a modification of the cloud drop number concentration in subsequent clouds [Feingold and Kreidenweis, 2000].

Sulfate formation in fogs has long been considered to contribute to acidification of rain [Jacob and Hoffmann, 1983]. In-cloud sulfate formation is known as the major source of global sulfate [Barth et al., 2000; Ervens, 2015 and references therein] because aqueous-phase oxidation of sulfur(IV) by hydrogen peroxide and ozone occurs much more rapidly than gas phase oxidation by OH [Seinfeld and Pandis, 2006]. Kinetic and mechanistic data for the oxidation of sulfur(IV) are relatively well constrained; however, sulfate formation depends

not only upon chemical parameters such as pH and the availability of oxidants (H_2O_2 and O_3) but also upon microphysical cloud parameters such as liquid water content (LWC) and droplet lifetime [Ervens, 2015]. Uncertainties in cloud properties due to measurements or parameterizations translate into uncertainties in predicted concentrations of sulfate [e.g., Berg *et al.*, 2015; Koch *et al.*, 2003] and also, in general, of other chemical species [Barth *et al.*, 2007]. Since sulfate aerosols play an important role in both the indirect and direct aerosol effects [Chin *et al.*, 2000; Chuang and Penner, 1995; Chuang *et al.*, 1997; Easter and Hobbs, 1974; Lee *et al.*, 2013; Myhre *et al.*, 2004; Yuen *et al.*, 1994], cloud properties and in-cloud sulfate production both have to be accurately constrained in order to predict aerosols' influence on radiative forcing.

Small fog and cloud droplets are usually more acidic than larger ones [Collett *et al.*, 1994]. The pH affects the solubility of SO_2 and strongly affects the aqueous-phase sulfur(IV) oxidation rates for ozone reactions and to a smaller extent H_2O_2 reactions [Seinfeld and Pandis, 2006], which leads to size-dependent sulfate formation rates throughout drop populations [Moore *et al.*, 2004]. Changes in aerosol distributions due to sulfate chemistry have been explored in different model configurations [Ovchinnikov and Easter, 2010]. This pH effect has been implemented to some extent into chemical transport models [Fahey and Pandis, 2003; Roelofs, 1992]. However, in most regional and global models, simplifying assumptions are employed, such as using only one drop size, assuming thermodynamic equilibrium between gas and aqueous phases (Henry's law), or predicting sulfate formation based on empirical expressions [Ervens, 2015, and references therein].

Secondary organic aerosol (SOA), formed via gas-to-particle conversion, has been recognized as a major contributor to total particle mass [Kanakidou *et al.*, 2005; Turpin and Huntzicker, 1995]. Historically, the focus has been on "traditional" SOA, formed when volatile organic compounds react in the gas phase to form low-volatility products, which then partition to the particle phase [Pankow, 1994]. Parameterizations have been suggested to efficiently model traditional SOA, such as the two-product model [Odum *et al.*, 1996] or the volatility basis set [Donahue *et al.*, 2011; Shrivastava *et al.*, 2017].

More recently, aqSOA has been suggested to contribute to particle mass [Blando and Turpin, 2000]. Cloud aqSOA formation occurs when water-soluble organics undergo chemical reactions in the aqueous phase of cloud droplets to form highly oxygenated products that remain in the particle upon water evaporation [e.g., Ervens *et al.*, 2011; Lim *et al.*, 2010]. AqSOA can also be formed in more concentrated solutions typical of deliquesced aerosols (aerosol aqSOA) [e.g., Galloway *et al.*, 2011; Nguyen *et al.*, 2012], but we focus here only on dilute conditions as encountered in clouds. Cloud aqSOA formation typically proceeds via OH oxidation; although OH is less soluble than other oxidants, such as hydrogen peroxide, its rate constant with organics is much higher, leading to more efficient aqSOA formation rates [Ervens *et al.*, 2003; Schöne and Herrmann, 2014].

The description of cloud aqSOA formation is computationally more complex to represent than traditional SOA formation because chemical concentrations in both aqueous and gas phases have to be tracked simultaneously, together with cloud properties. The description of organic oxidation in the gas phase is computationally expensive as the number of chemical species increases exponentially with the number of C atoms [Aumont *et al.*, 2005]. Explicit oxidation mechanisms for aqueous organics are also available; however, these mechanisms are similarly complex and include tens to hundreds of species [Ervens *et al.*, 2003; Herrmann *et al.*, 2000; Mouchel-Vallon *et al.*, 2013].

Different approaches have been used to simplify the representation of cloud aqSOA chemistry. Condensed mechanisms include lumped processes or compounds to reduce the number of species [e.g., Deguillaume *et al.*, 2009; Ervens *et al.*, 2003; Woo and McNeill, 2015]. In global simulations of in-cloud mass formation, reduced aqueous-phase mechanisms have been used with a fixed droplet radius of 5 (or 6) μm over land and 10 μm over oceans [Myriokefalitakis *et al.*, 2011; Roelofs *et al.*, 1998]. Other, more empirical, aqSOA parameterizations use LWC [Ervens *et al.*, 2008], surface [Fu *et al.*, 2009], or simple yields [Carlton *et al.*, 2008]; however, these parameterizations are often based on single lab experiments or on experiments conducted under atmospherically irrelevant conditions.

AqSOA formation is drop size dependent [Chakraborty *et al.*, 2016]; trends of increasing oxalate mass with increasing drop surface area have been predicted based on process models and identified in field data [Ervens *et al.*, 2014]. This size dependence results from oxidant limitation; because of its low solubility and high reactivity, aqueous OH is limited by surface uptake [Ervens *et al.*, 2003, 2014]. This limitation is

manifested as a size dependence of aqSOA formation. However, using prognostic approaches, modeling more than one droplet size increases the number of variables even further because aqueous species in each droplet class are tracked separately [Ghan and Easter, 2006], and the total number of aqueous-phase species is the product of the number of dissolved chemical species and the number of droplet classes. Tracking this many variables is nearly impossible for models; therefore, often, the sulfate mass is distributed based on various diagnostic approaches that do not require that many variables and, thus, computational power.

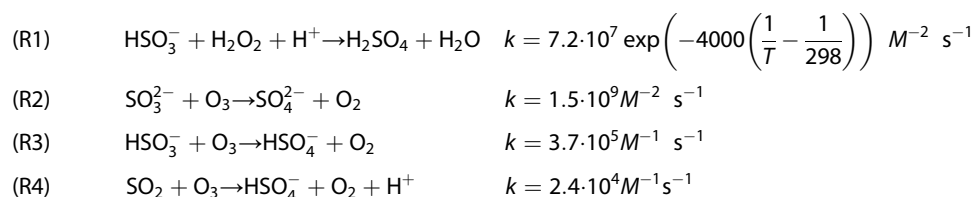
None of the previous parameterizations systematically includes the observed and predicted drop size dependence of cloud aqSOA formation, whereas corresponding studies have been performed for sulfate [e.g., Ovchinnikov and Easter, 2010]. The most accurate representation of aqSOA should therefore be based on actual cloud drop size distributions. However, these size distributions are often not available from measurements and poorly (if at all) represented in models.

The aim of the present study is to develop a reliable and efficient way to parameterize cloud aqSOA and sulfate formation by reducing the number of microphysical variables (drop size classes) while maintaining the surface and size dependence of sulfate and aqSOA formation. We investigate methods of parameterizing the aqSOA and sulfate mass formation rates in cloud drop size distributions with a single class size that reproduces the formation rates in the original polydisperse cloud droplet population.

2. Model Description

2.1. Box Model

The box model describes both aqSOA (oxidation of glyoxal) and sulfate formation. It consists of the aqueous-phase chemical mechanism for glyoxal oxidation given in Lim *et al.* [2010] and aqueous-phase reactions for sulfate formation:



The mechanism consists of 20 water-soluble gas-phase species and 30 aqueous-phase species without a counterpart in the gas phase. Partitioning between the gas and aqueous phases is based on mass accommodation coefficients, gas-phase diffusion, and Henry's law constants [Ervens *et al.*, 2004]. Each simulation is initialized with 1 ppb glyoxal, $5 \cdot 10^6 \text{ cm}^{-3}$ OH, 0.1 ppb H_2O_2 , 60 ppb O_3 , and 1 ppb SO_2 that remain constant throughout the 1 h simulations, together with temperature (298 K), pressure (1 atm), and relative humidity (~100%).

2.1.1. Polydisperse Distribution

The drop size distribution contains 20 logarithmically spaced drop size classes (0.25–40 μm) and does not change over the course of a model run. The median droplet diameter D_g , standard deviation σ_g , and total droplet number concentration N_{dr} are varied between simulations leading to different total LWCs.

Base simulations were performed with identical pH across all size classes (varying pH between simulations); sensitivity tests were performed with a size-dependent pH distribution. For these sensitivity tests, the pH was varied by one unit across the 20 size classes (e.g., between 4 and 5), with smallest droplets being most acidic [Collett *et al.*, 1994].

2.1.2. Monodisperse Distribution

For each combination of D_g , σ_g , N_{dr} , and pH, a single-size class version of the model was run to attempt to reproduce the same overall aqSOA and sulfate formation rates as in the polydisperse simulation. Different single diameters are tested for the monodisperse model, and N_{dr} is adjusted to maintain the total LWC of the corresponding polydisperse simulation. The LWC was chosen to match in the monodisperse version because this parameter is usually well constrained by measurements and predicted in cloud models.

An overview of the different simulations for each combination of parameters (D_g , σ_g , and N_{dr}) and pH is shown in the upper part of Table 1. Tested single diameters include D_g from the corresponding full-size distribution (SB#2) and ratios of different moments from the full droplet size distribution: the ratio of the fourth

Table 1. Description of Simulations Run for Each Combination of Size Distribution Parameters and pH Value^a

Simulation	Description	Diameter
SB#1	Full-size distribution (20 drop size classes)	Variable D 's based on D_g and σ_g
SB#2	Single-size class: median diameter of the full-size distribution	D_g
SB#3	Single-size class: the ratio of the fourth to third moment	$D_{4/3}$
SB#4	Single-size class: the effective diameter (ratio of the third to second moment)	D_{eff}
SB#5	Single-size class: the ratio of the second to first moment	$D_{2/1}$
SP#1	Full-size distribution (10 drop size classes)	Variable D 's based on D_g and σ_g
SP#2	Single-size class: time-dependent effective diameter	$D_{\text{eff},t}$
SP#3	Single-size class: average of the time-dependent effective diameter	$D_{\text{eff,av}}$
SP#4	Single-size class: 5 μm	D_5
SP#5	Single-size class: 10 μm	D_{10}

^aSB simulations refer to the box model, and SP simulations refer to the parcel model.

to third moment (SB#3), the ratio of the third to second moment (SB#4), and the ratio of the second to first moment (SB#5) to reflect complex trends in terms of a combination of surface and volume dependencies.

The ratio of the third to second moment is known as the effective diameter D_{eff} [Hansen and Travis, 1974]:

$$D_{\text{eff}} = \frac{\sum_j (N_j (D_j)^3)}{\sum_j (N_j (D_j)^2)} \quad (1)$$

with D_j and N_j diameter and number concentration of size class j . It is proportional to the volume-to-surface area ratio of a full-size distribution.

Since the polydisperse distribution remains constant throughout a simulation, the representative diameter for a monodisperse simulation also remains constant. For base simulations, pH is set to the same value as in the polydisperse simulation. For sensitivity studies using a size-dependent pH distribution, the volume-averaged H^+ concentration is calculated for the polydisperse distribution. The pH for the corresponding monodisperse simulation is set to the base-10 logarithm of this volume-averaged H^+ concentration.

To compare the performance of a single class to the corresponding full-size distribution simulation, the ratio of the aqSOA or sulfate concentrations at the conclusion of each 1 h simulation is calculated:

$$R = \frac{m_{\text{single}}}{m_{\text{full}}} \quad (2)$$

where m_{single} the mass of aqSOA or sulfate for any of SB2–SB#5 and m_{full} the mass of aqSOA or sulfate for SB#1. A perfect match between the mass formation rates in the polydisperse and monodisperse distributions results in R of unity. We refer to the ratios for aqSOA and sulfate as R_{aqSOA} and R_{Sulf} , respectively.

2.2. Cloud Parcel Model

The box model, with constant temperature, relative humidity, and LWC, provides a useful framework to explore trends and sensitivities in aqSOA and sulfate formation. However, it is necessary to verify the robustness of these trends in more realistic, variable cloud conditions that reflect the growth and evaporation of cloud droplets, for which we apply the cloud parcel model.

2.2.1. Polydisperse Cloud Droplet Distribution

The cloud parcel model has been described previously [Ervens et al., 2004; Feingold and Heymsfield, 1992; Feingold et al., 1998]. In brief, in contrast to the box model, the parcel model is initialized with a population of unactivated, deliquesced ammonium sulfate particles apportioned into 10 logarithmically spaced size classes (0.01–1 μm), with different initial D_g , σ_g , and aerosol number concentration N_a between simulations. The initial relative humidity is between 56 and 89%, and thus, particles contain some initial water.

The aerosol particles are exposed to a trajectory describing the path of an air parcel through shallow cumulus or stratocumulus clouds. A total of 505 different trajectories are used to examine aqSOA and sulfate formation in shallow cumulus and stratocumulus clouds [Ervens et al., 2008; Wonaschuetz et al., 2012]. The in-cloud time of each parcel is on the order of 5–10 min for shallow cumulus and 20–40 min for stratocumulus clouds.

As the temperature, pressure, and relative humidity change along the trajectory, the particles take up water vapor and are activated into cloud droplets according to Köhler theory. The chemical mechanism and constant gas-phase concentrations are the same as in the box model, representing the formation of cloud aqSOA from glyoxal and of aqueous sulfate. Aqueous-phase chemistry in the individual size classes starts when total LWC surpasses 10^{-6} g/g and when total solute concentrations of $[\text{SO}_4^{2-}] + [\text{NH}_4^+]$ in an individual size class falls below 1 M. As the air parcel passes out of the cloud, water evaporates and the droplets deactivate, while aqSOA and sulfate remain in the particles [Ervens *et al.*, 2004].

The pH is considered to be the same in each initial aerosol size class and does not change once the particles get activated in the cloud. Sensitivity tests were conducted using a size-dependent pH distribution. The simplifying assumption of a constant pH throughout the lifetime of a droplet can be justified as in reality droplets are diluted during growth but may also take up acidic/basic gases (or their precursors) so that the initial trend in pH values remains similar. Change in pH due to uptake of gases is not explicitly simulated in our model.

2.2.2. Monodisperse Cloud Droplet Distribution

Again, model simulations using polydisperse distributions were compared to those using only a single-size class. A description of all simulations run for each trajectory and size distribution is shown in the bottom part of Table 1. Because the LWC for a polydisperse simulation changes as the air parcels pass into and out of clouds while droplets grow and evaporate, the LWC for the corresponding monodisperse simulation has to be adjusted accordingly. Again, different single diameters are tested for the single-class simulation. N_a is artificially changed in the model cloud such that the time-dependent LWC from the full-size distribution is reproduced. While such a change in particle number is rather unrealistic, we chose this approach so that the LWC remains the same between the monodisperse and polydisperse simulations. In the monodisperse simulations, we do not consider explicit aerosol activation but use the derived time-dependent, monodisperse drop number concentration that reproduces the identical LWC as in the polydisperse simulations.

Based on box model results, only four representative diameters are tested: time-dependent D_{eff} of the full-size distribution simulation ($D_{\text{eff},i}$; SP#2) and three constant diameters: the average of D_{eff} ($D_{\text{eff},av}$; SP#3), 5 μm (D_5 , SP#4), and 10 μm (D_{10} , SP#5). The values for SP#4 and SP#5 were chosen similar to the assumptions made in global models [Myriokefalitakis *et al.*, 2011; Roelofs *et al.*, 1998].

To calculate $D_{\text{eff},t}$ according to equation (1), the time-dependent total LWC and droplet surface area are recorded for each trajectory using the polydisperse distribution (see Figure S1 in the supporting information for an example trajectory). $D_{\text{eff},t}$ is only calculated in cloud when $\text{LWC} > 10^{-6}$ g/g and changes gradually from 0 to 11 μm . The average value of $D_{\text{eff},t}$ between cloud base and cloud top represents the constant $D_{\text{eff},av}$ which is presented by a step function between 0 and ~ 9.2 μm and is also calculated for each initial aerosol size distribution and trajectory.

For SP#1 simulations using a size-independent pH, the pH for all monodisperse simulations SP#2–SP#5 is set to the same value (pH = 1, 3, 5, or 7). For additional sensitivity tests using a size-dependent pH distribution, the pH was calculated differently than in the box model simulations since not all size classes are activated. Thus, using the volume-averaged H^+ concentration assigned to the initial aerosol size distribution may not accurately represent the true volume-averaged concentration in cloud. Therefore, we recorded the volume-averaged H^+ concentration for SP#1, which starts with relatively high pH when the largest particles activate and decreases successively when the smaller size classes (with lower pH) activate. When pH is varied by one unit across the 10 size classes (e.g., 4 to 5 from the smallest to the largest particle), the volume-averaged pH ranged from 4.4 to 4.7, depending on the parameters of the initial size distribution (σ_g and D_g). Because the spread of pH values throughout the drop population is typically not known from measurements and because it would be too complex to be represented in models, we assumed a constant pH of two thirds of the pH range (e.g., 4.6) to use in the single-size class simulations.

3. Results and Discussion

3.1. Box Model

3.1.1. R_{aqSOA}

Figures 1a–1d show R_{aqSOA} for SB#2–SB#5 for a range of size distribution parameters. For very narrow distributions ($\sigma_g \sim 1.1$), R_{aqSOA} is near unity for all SB#2–SB#5.

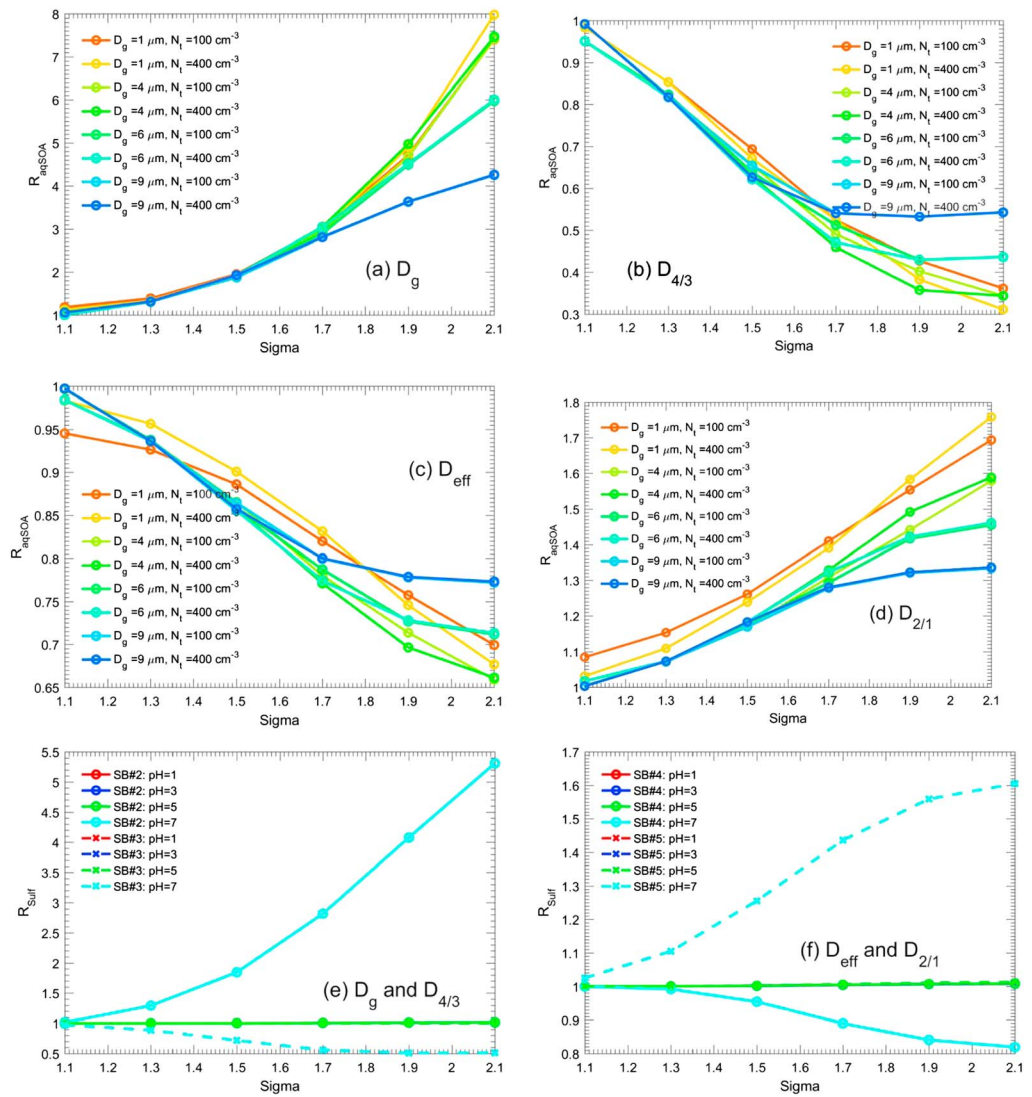


Figure 1. R_{aqSOA} and R_{Sulf} as a function of σ_g . Six values of σ_g were used for each combination of parameters. Lines are only added to guide the eye. (a) R_{aqSOA} for SB#2, (b) R_{aqSOA} for SB#3, (c) R_{aqSOA} for SB#4, (d) R_{aqSOA} for SB#5, (e) R_{Sulf} for SB#2 and SB#3, and (f) R_{Sulf} for SB#4 and SB#5. Note that the results for pH = 1, 3, and 5, respectively, are on top of each other in Figures 1e and 1f.

For broad size distributions, SB#4 (D_{eff} ; Figure 1c) performs better than the other single-class simulations by a substantial margin: R_{aqSOA} for SB#2 (Figure 1c) ranges as high as 8 for large σ_g , as opposed to 0.65 for SB#4, meaning that using D_g leads to an overestimate of aqSOA mass by 700%, whereas using D_{eff} results in an underestimate of only ~30%. For SB#2–SB#5, percent differences increase with increasing σ_g but are relatively unaffected by D_g or N_{dr} .

The decreasing performance of a single-size class with increasing σ_g is expected; as a size distribution broadens, a single-size class introduces more bias at reproducing the mass formation rate in polydisperse drop population.

Based on these simulations, we conclude that D_{eff} (SB#4) is a reasonable representation to predict aqSOA concentrations for a full-size class simulation. Ratios of other moments (fourth/third and second/first) perform worse on average (SB#3 and SB#5 in Figures 1b and 1d, respectively). The superior performance of D_{eff} over the other assumed approximations for a single D can be explained by the strong surface area dependence of aqSOA formation and the inverse relationship of aqSOA mass with volume (LWC) that has been discussed previously [Ervens et al., 2014].

3.1.2. R_{aqSulf}

R_{Sulf} was equivalently calculated for SB#2–SB#5. Previous studies have shown that sulfate formation is not (strongly) dependent on drop surface area [Ervens *et al.*, 2014] but it is dependent on pH due to the strong increase in rate constants with increasing contribution of HSO_3^- and SO_3^{2-} to total sulfur(IV) (R2–R4). Therefore, Figures 1e and 1f show R_{Sulf} as a function of σ_g for a range of pH values using a single, constant pH throughout the size distribution for various simulations.

For $\text{pH} \leq 5$, SB#2–SB#5 perform equivalently at predicting sulfate concentrations, with virtually no dependence on σ_g . This trend is expected as sulfate formation at this pH range is mostly driven by the S(IV) oxidation by H_2O_2 . The uptake of highly soluble H_2O_2 is not limited by the available drop surface area, and thus, LWC is the major parameter that determines the overall sulfate formation rate in cloud water. At $\text{pH} = 7$, when sulfate is mostly formed by R4, SB#4 (D_{eff}) gives the best agreement with the full-size distribution simulation, since the low solubility of O_3 ($K_H = 0.014 \text{ M atm}^{-1}$) [Weinstein-Lloyd and Schwartz, 1991] limits its uptake and thus the drop size distribution determines the oxidation rate. At high pH, increasing σ_g results in worse agreement for all SB#2–SB#5. These results suggest that sulfate formation becomes dependent on surface area only at very high pH values, at which the rate of sulfate formation will be highest due to the increasing pH sensitivity with increasing pH of R2–R4 [Seinfeld and Pandis, 2006].

These simulations also demonstrate that any choice of a single diameter is likely sufficient to represent sulfate formation at $\text{pH} \leq \sim 6$ as usually encountered in the atmosphere. For fully neutralized cloud water, the use of D_{eff} (SB#4) should be preferred.

Sensitivity tests of the pH effect were performed for SB#1, in which the pH was varied by one unit across the 20 size classes (2–3, 4–5, and 6–7), with smallest classes being most acidic. The pH for SB#2–SB#5 was set to the logarithm of the volume-averaged H^+ concentration in the full-size distribution. R_{Sulf} values (not shown) display equivalent trends to those shown in Figures 1e and 1f for SB#2–SB#5, indicating that the conclusions are robust even when pH varies moderately across a size distribution.

3.2. Cloud Parcel Model

To test if these conclusions from the box model extrapolate to more realistic conditions in a growing and evaporating cloud, corresponding simulations are performed using a parcel model. We compare the full-size distribution simulation (SP#1) with four representative diameters in the single-class simulations (SP#2–SP#5, bottom part of Table 2).

Figure 2 shows predicted aqSOA and sulfate masses in a stratocumulus cloud trajectory for SP#1–SP#5 using $N_a = 100 \text{ cm}^{-3}$, $\sigma_g = 2.1$, and $\text{pH} = 5$ (constant). For aqSOA, SP#2 gives nearly perfect agreement with SP#1 ($R_{\text{aqSOA}} = 0.99$), whereas SP#3 and SP#5 give reasonable agreement ($R_{\text{aqSOA}} = 1.4$ and $R_{\text{aqSOA}} = 2.2$, respectively), but the arbitrary single diameter of $5 \mu\text{m}$ (SP#4) results in significant overprediction ($R_{\text{aqSOA}} = 7.9$). For sulfate, all single-class simulations give nearly the same good agreement with SP#1, in agreement with our findings from the box model simulations.

Results of additional sensitivity studies for wide ranges of σ_g , D_g , N_a , pH, and trajectories are summarized in Tables S1 (aqSOA) and S2 (sulfate). Generally, R_{aqSOA} ranges between 0.97 and 1.0 for SP#2 ($D_{\text{eff},t}$), between 1.1 and 1.2 for SP#3 ($D_{\text{eff,av}}$), between 3.3 and 12.8 for SP#4 (D_5), and between 0.94 and 3.6 for SP#5 (D_{10}). As seen in the box model studies already, for aqSOA, the use of D_{eff} (either as time-dependent or averaged value) gives the best agreement. This result signifies that the use of constant diameters of, e.g., 5 or $10 \mu\text{m}$ diameter, likely does not accurately capture the formation of aqSOA for most cloud droplet size distributions and that the use of $D_{\text{eff},t}$ or $D_{\text{eff,av}}$ is a significant improvement.

For aqueous sulfate, all diameters perform roughly equivalently as approximations for the full-size distribution (R_{Sulf} ranges from 1.1 to 1.2 regardless of SP#2–SP#5) for $1 < \text{pH} < 5$ (constant in all size classes and time independent). R_{Sulf} for additional sensitivity tests for pH ranges of one unit across the droplet distribution are shown in Table S3. For pH ranges of 2 to 3 or 4 to 5 from smallest to largest particle (droplet) sizes, R_{Sulf} ranges from 1.1 to 1.2 regardless of SP#2–SP#5, similar to results from size-independent pH simulations. For a higher pH values ($6 < \text{pH} < 7$), R_{Sulf} ranges from 1.5 to 3.1. For this pH range, SP#2 and SP#3 provide the best agreement. These simulations demonstrate, in agreement with the box model, that sulfate formation is rather insensitive to cloud parameters and any choice of diameter is sufficient to

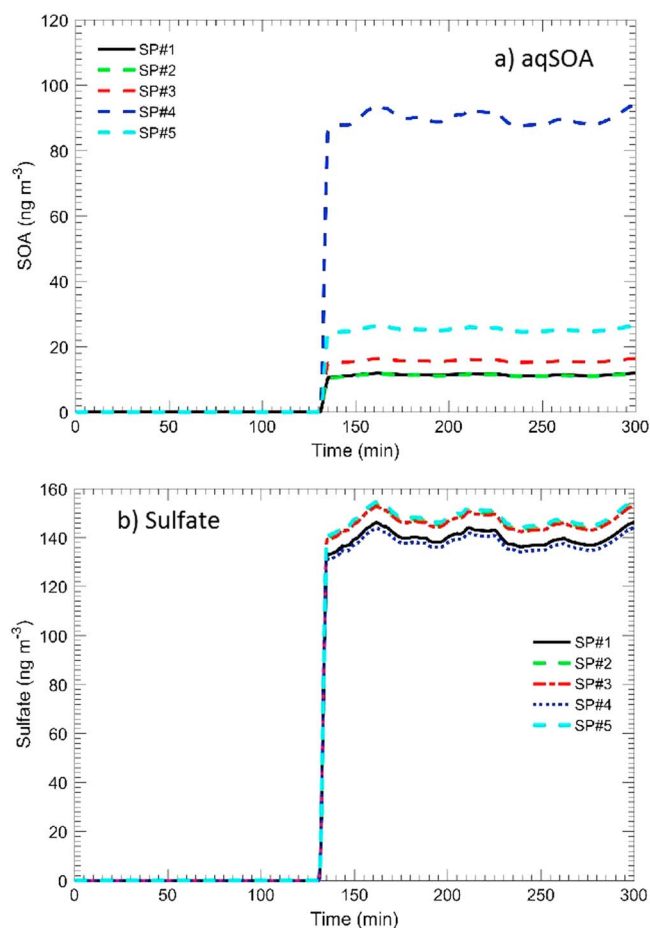


Figure 2. (a) AqSOA and (b) sulfate predictions as a function of time for an example cumulus cloud trajectory. Predictions are shown from the full-size distribution model (SP#1) as well as four cases of the single-size class model: SP#2–SP#5. The size distribution for these simulations has $N_0 = 100 \text{ cm}^{-3}$ and $\sigma_g = 2.1$ and $\text{pH} = 5$.

Our cloud cases are idealized and only assume monomodal, logarithmically spaced drop (or initial particle) size distributions, it can be expected that the findings are robust for other situations, e.g., for bimodal distributions or when the effective diameter is not as continuous in a cloud due to entrainment. Thus, D_{eff} represents a computationally inexpensive way to improve the accuracy of cloud aqSOA and sulfate predictions in regional and global models. This microphysical parameterization can be included into models using reduced chemical mechanisms so that the overall number of variables for aqueous-phase chemistry (i.e., the product of dissolved chemical species and droplet size classes) is further decreased. Our simulations clearly show that using D_{eff} rather than an assumed fixed diameter, as it has been done previously in chemical transport or global models, preserves the sensitivity of aqSOA formation to the surface-to-volume ratio. Other approaches, such as empirical parameterizations, are often not fully able to represent the feedbacks of drop surface area and volume dependencies of sulfate and, in particular, aqSOA formation.

D_{eff} is frequently measured or estimated for clouds, using in situ aircraft measurements, satellite retrievals [e.g., Painemal and Zuidema, 2011], or parameterizations based on cloud parameters [Martin et al., 1994]. It is used to estimate liquid water path and cloud droplet number concentration [e.g., Bennartz, 2007]. Since D_{eff} or its proxies can be derived from measurements and is used routinely in models (e.g., for radiation calculations), it seems straightforward to pass it to the subroutines that include the description of in-cloud sulfate and aqSOA formation.

represent sulfate formation at common pH values and ranges; a at $\text{pH} > \sim 6$, the effective diameter (SP#2 or SP#3) should be preferred.

4. Conclusions

The average effective diameter ($D_{\text{eff,av}}$) is a reasonable representation of a polydisperse distribution for aqSOA and sulfate formation in clouds, with only small improvement if a time-dependent effective diameter ($D_{\text{eff,t}}$) is used. This result was suggested empirically for oxalate formation [Ervens et al., 2014] as it takes into account the complex dependency of OH-driven chemistry on both surface area and volume. In that study, oxalate did not correlate with LWC unless also sorted by drop surface area, indicating a dependence on both LWC and drop surface area. Furthermore, although sulfate formation is typically not size dependent and can be represented by any diameter, we find that at $\text{pH} > 5$, D_{eff} is the most accurate representation of a full-size distribution.

The use of the single, effective diameter rather than a full-size distribution dramatically lowers the computational cost of simulations; in our cloud parcel model, the single-class simulation was ~ 18 times faster than the polydisperse simulation. While our

Unlike other parameterizations of aqueous phase chemistry, this parameterization reduces the microphysical rather than the chemical parameters, allowing chemical complexity to be preserved (and potentially expanded to include other aqSOA formation pathways) without excessive computational expense.

Acknowledgments

The authors acknowledge support by NOAA's climate goal. R.M. was supported by a CIRES Visiting Fellowship. The model simulation output can be accessed at <https://esrl.noaa.gov/csd/groups/csd2/clouds>.

References

- Aumont, B., S. Szopa, and S. Madronich (2005), Modelling the evolution of organic carbon during its gas-phase tropospheric oxidation: Development of an explicit model based on a self-generating approach, *Atmos. Chem. Phys.*, *5*(9), 2497–2517, doi:10.5194/acp-5-2497-2005.
- Barth, M. C., P. J. Rasch, J. T. Kiehl, C. M. Benkovitz, and S. E. Schwartz (2000), Sulfur chemistry in the National Center for Atmospheric Research Community Climate Model: Description, evaluation, features, and sensitivity to aqueous chemistry, *J. Geophys. Res.*, *105*, 1387–1415, doi:10.1029/1999JD900773.
- Barth, M. C., et al. (2007), Cloud-scale model intercomparison of chemical constituent transport in deep convection, *Atmos. Chem. Phys.*, *7*(18), 4709–4731, doi:10.5194/acp-7-4709-2007.
- Bennartz, R. (2007), Global assessment of marine boundary layer cloud droplet number concentration from satellite, *J. Geophys. Res.*, *112*, D02201, doi:10.1029/2006JD007547.
- Berg, L. K., M. Shrivastava, R. C. Easter, J. D. Fast, E. G. Chapman, Y. Liu, and R. A. Ferrare (2015), A new WRF-Chem treatment for studying regional-scale impacts of cloud processes on aerosol and trace gases in parameterized cumuli, *Geosci. Model Dev.*, *8*(2), 409–429, doi:10.5194/gmd-8-409-2015.
- Blando, J. D., and B. J. Turpin (2000), Secondary organic aerosol formation in cloud and fog droplets: A literature evaluation of plausibility, *Atmos. Environ.*, *34*, 1623–1632.
- Carlton, A. G., B. J. Turpin, K. E. Altieri, S. P. Seitzinger, R. Mathur, S. J. Roselle, and R. J. Weber (2008), CMAQ model performance enhanced when in-cloud secondary organic aerosol is included: Comparisons of organic carbon predictions with measurements, *Environ. Sci. Technol.*, *42*(23), 8789–8802.
- Chakraborty, A., B. Ervens, T. Gupta, and S. N. Tripathi (2016), Characterization of organic residues of size-resolved fog droplets and their atmospheric implications, *J. Geophys. Res. Atmos.*, *121*, 4317–4332, doi:10.1002/2015JD024508.
- Chin, M., R. B. Rood, S.-J. Lin, J.-F. Müller, and A. M. Thompson (2000), Atmospheric sulfur cycle simulated in the global model GOCART: Model description and global properties, *J. Geophys. Res.*, *105*, 24,671–24,687, doi:10.1029/2000JD900384.
- Chuang, C. C., and J. E. Penner (1995), Effects of anthropogenic sulfate on cloud drop nucleation and optical properties, *Tellus Ser. B Chem. Phys. Meteorol.*, *47*(5), 566–577, doi:10.3402/tellusb.v47i5.16072.
- Chuang, C. C., J. E. Penner, K. E. Taylor, A. S. Grossman, and J. J. Walton (1997), An assessment of the radiative effects of anthropogenic sulfate, *J. Geophys. Res.*, *102*, 3761–3778, doi:10.1029/96JD03087.
- Collett, J. L., A. Bator, X. Rao, and B. B. Demoz (1994), Acidity variations across the cloud drop size spectrum and their influence on rates of atmospheric sulfate production, *Geophys. Res. Lett.*, *21*, 2393–2396, doi:10.1029/94GL02480.
- Deguillaume, L., A. Tilgner, R. Schrödner, R. Wolke, N. Chaumerliac, and H. Herrmann (2009), Towards an operational aqueous phase chemistry mechanism for regional chemistry-transport models: CAPRAM-RED and its application to the COSMO-MUSCAT model, *J. Atmos. Chem.*, *64*(1), 1–35, doi:10.1007/s10874-010-9168-8.
- Donahue, N. M., S. A. Epstein, S. N. Pandis, and A. L. Robinson (2011), A two-dimensional volatility basis set: 1. Organic-aerosol mixing thermodynamics, *Atmos. Chem. Phys.*, *11*(7), 3303–3318, doi:10.5194/acp-11-3303-2011.
- Easter, R. C., and P. V. Hobbs (1974), The formation of sulfates and the enhancement of cloud condensation nuclei in clouds, *J. Atmos. Sci.*, *31*(6), 1586–1594, doi:10.1175/1520-0469(1974)031<1586:tfosat>2.0.co;2.
- Ervens, B. (2015), Modeling the processing of aerosol and trace gases in clouds and fogs, *Chem. Rev.*, *115*(10), 4157–4198, doi:10.1021/cr5005887.
- Ervens, B., A. G. Carlton, B. J. Turpin, K. E. Altieri, S. M. Kreidenweis, and G. Feingold (2008), Secondary organic aerosol yields from cloud-processing of isoprene oxidation products, *Geophys. Res. Lett.*, *35*, L02816, doi:10.1029/2007GL031828.
- Ervens, B., G. Feingold, G. J. Frost, and S. M. Kreidenweis (2004), A modeling study of aqueous production of dicarboxylic acids: 1. Chemical pathways and speciated organic mass production, *J. Geophys. Res.*, *109*, D15205, doi:10.1029/2003JD004387.
- Ervens, B., et al. (2003), CAPRAM2.4 (MODAC mechanism): An extended and condensed tropospheric aqueous phase mechanism and its application, *J. Geophys. Res.*, *108*(D14), 4426, doi:10.1029/2002JD002202.
- Ervens, B., A. Sorooshian, Y. B. Lim, and B. J. Turpin (2014), Key parameters controlling OH-initiated formation of secondary organic aerosol in the aqueous phase (aqSOA), *J. Geophys. Res. Atmos.*, *119*, 3997–4016, doi:10.1002/2013JD021021.
- Ervens, B., B. J. Turpin, and R. J. Weber (2011), Secondary organic aerosol formation in cloud droplets and aqueous particles (aqSOA): A review of laboratory, field and model studies, *Atmos. Chem. Phys.*, *11*(21), 11,069–11,102, doi:10.5194/acp-11-11069-2011.
- Fahey, K. M., and S. N. Pandis (2003), Size-resolved aqueous-phase atmospheric chemistry in a three-dimensional chemical transport model, *J. Geophys. Res.*, *108*(D22), 4690, doi:10.1029/2003JD003564.
- Feingold, G., and A. J. Heymsfield (1992), Parameterizations of condensational growth of droplets for use in general circulation models, *J. Atmos. Sci.*, *49*(23), 2325–2342, doi:10.1175/1520-0469(1992)049<2325:pocgod>2.0.co;2.
- Feingold, G., and S. Kreidenweis (2000), Does cloud processing of aerosol enhance droplet concentrations?, *J. Geophys. Res.*, *105*, 24,351–24,361, doi:10.1029/2000JD900369.
- Feingold, G., S. M. Kreidenweis, and Y. P. Zhang (1998), Stratocumulus processing of gases and cloud condensation nuclei: 1. Trajectory ensemble model, *J. Geophys. Res.*, *103*, 19,527–19,542, doi:10.1029/98JD01750.
- Fu, T., D. J. Jacob, and C. L. Heald (2009), Aqueous-phase reactive uptake of dicarbonyls as a source of organic aerosol over eastern North America, *Atmos. Environ.*, *43*, 1814–1822.
- Galloway, M. M., C. L. Loza, P. S. Chhabra, A. W. H. Chan, L. D. Yee, J. H. Seinfeld, and F. N. Keutsch (2011), Analysis of photochemical and dark glyoxal uptake: Implications for SOA formation, *Geophys. Res. Lett.*, *38*, L17811, doi:10.1029/2011GL048514.
- Ghan, S. J., and R. C. Easter (2006), Impact of cloud-borne aerosol representation on aerosol direct and indirect effects, *Atmos. Chem. Phys.*, *6*(12), 4163–4174, doi:10.5194/acp-6-4163-2006.
- Hansen, J. E., and L. D. Travis (1974), Light-scattering in planetary atmospheres, *Space Sci. Rev.*, *16*(4), 527–610, doi:10.1007/bf00168069.
- Herrmann, H., B. Ervens, H. W. Jacobi, R. Wolke, P. Nowacki, and R. Zellner (2000), CAPRAM2.3: A chemical aqueous phase radical mechanism for tropospheric chemistry, *J. Atmos. Chem.*, *36*(3), 231–284, doi:10.1023/a:1006318622743.

- Intergovernmental Panel on Climate Change (2013), Fifth assessment report, climate Change Rep., Intergovernmental Panel on Climate Change.
- Jacob, D. J., and M. R. Hoffmann (1983), A dynamic model for the production of H^+ NO_3^- , and SO_4^{2-} in urban fog, *J. Geophys. Res.*, *88*, 6611–6621, doi:10.1029/JC088iC11p06611.
- Kanakidou, M., et al. (2005), Organic aerosol and global climate modelling: A review, *Atmos. Chem. Phys.*, *5*, 1–70.
- Koch, D., J. Park, and A. Del Genio (2003), Clouds and sulfate are anticorrelated: A new diagnostic for global sulfur models, *J. Geophys. Res.*, *108*(D24), 4781, doi:10.1029/2003JD003621.
- Lee, L. A., K. J. Pringle, C. L. Reddington, G. W. Mann, P. Stier, D. V. Spracklen, J. R. Pierce, and K. S. Carslaw (2013), The magnitude and causes of uncertainty in global model simulations of cloud condensation nuclei, *Atmos. Chem. Phys.*, *13*(17), 8879–8914, doi:10.5194/acp-13-8879-2013.
- Lim, Y. B., Y. Tan, M. J. Perri, S. P. Seitzinger, and B. J. Turpin (2010), Aqueous chemistry and its role in secondary organic aerosol (SOA) formation, *Atmos. Chem. Phys.*, *10*(21), 10,521–10,539, doi:10.5194/acp-10-10521-2010.
- Martin, G. M., D. W. Johnson, and A. Spice (1994), The measurement and parameterization of effective radius of droplets in warm stratocumulus clouds, *J. Atmos. Sci.*, *51*(13), 1823–1842, doi:10.1175/1520-0469(1994)051<1823:tmapoe>2.0.co;2.
- Moore, K., D. E. Sherman, J. E. Reilly, and J. L. Collett (2004), Drop-size dependent chemical composition in clouds and fogs: Part I. Observations, *Atmos. Environ.*, *38*, 1389–1402.
- Mouchel-Vallon, C., P. Brauer, M. Camredon, R. Valorso, S. Madronich, H. Herrmann, and B. Aumont (2013), Explicit modeling of volatile organic compounds partitioning in the atmospheric aqueous phase, *Atmos. Chem. Phys.*, *13*(2), 1023–1037, doi:10.5194/acp-13-1023-2013.
- Myhre, G., F. Stordal, T. F. Berglen, J. K. Sundet, and I. S. A. Isaksen (2004), Uncertainties in the radiative forcing due to sulfate aerosols, *J. Atmos. Sci.*, *61*(5), 485–498, doi:10.1175/1520-0469(2004)061<0485:uitrfd>2.0.co;2.
- Myriokefalitakis, S., K. Tsigaridis, N. Mihalopoulos, J. Sciare, A. Nenes, K. Kawamura, A. Segers, and M. Kanakidou (2011), In-cloud oxalate formation in the global troposphere: A 3-D modeling study, *Atmos. Chem. Phys.*, *11*(12), 5761–5782, doi:10.5194/acp-11-5761-2011.
- Nguyen, T. B., P. B. Lee, K. M. Updyke, D. L. Bones, J. Laskin, A. Laskin, and S. A. Nizkorodov (2012), Formation of nitrogen- and sulfur-containing light-absorbing compounds accelerated by evaporation of water from secondary organic aerosols, *J. Geophys. Res.*, *117*, D01207 doi:10.1029/2011JD016944.
- Odum, J. R., T. Hoffmann, F. Bowman, D. Collins, R. C. Flagan, and J. H. Seinfeld (1996), Gas/particle partitioning and secondary organic aerosol yields, *Environ. Sci. Technol.*, *30*(8), 2580–2585, doi:10.1021/es950943+.
- Ovchinnikov, M., and R. C. Easter (2010), Modeling aerosol growth by aqueous chemistry in a nonprecipitating stratiform cloud, *J. Geophys. Res.*, *115*, D14210, doi:10.1029/2009JD012816.
- Painemal, D., and P. Zuidema (2011), Assessment of MODIS cloud effective radius and optical thickness retrievals over the Southeast Pacific with VOCALS-REx in situ measurements, *J. Geophys. Res.*, *116*, D24206, doi:10.1029/2011JD016155.
- Pankow, J. F. (1994), An absorption-model of the gas aerosol partitioning involved in the formation of secondary organic aerosol, *Atmos. Environ.*, *28*(2), 189–193, doi:10.1016/1352-2310(94)90094-9.
- Roelofs, G. (1992), Drop size dependent sulfate distribution in a growing cloud, *J. Atmos. Chem.*, *14*(1–4), 109–118, doi:10.1007/bf00115227.
- Roelofs, G., J. Lelieveld, and L. Ganzeveld (1998), Simulation of global sulfate distribution and the influence on effective cloud drop radii with a coupled photochemistry sulfur cycle model, *Tellus, Ser. B*, *50*(3), 224–242, doi:10.1034/j.1600-0889.1998.t01-2-00002.x.
- Schöne, L., and H. Herrmann (2014), Kinetic measurements of the reactivity of hydrogen peroxide and ozone towards small atmospherically relevant aldehydes, ketones and organic acids in aqueous solutions, *Atmos. Chem. Phys.*, *14*(9), 4503–4514, doi:10.5194/acp-14-4503-2014.
- Seinfeld, J. H., and S. N. Pandis (2006), *Atmospheric Chemistry and Physics: From Air Pollution to Climate Change*, John Wiley, Hoboken, N. J.
- Shrivastava, M., et al. (2017), Recent advances in understanding secondary organic aerosol: Implications for global climate forcing, *Rev. Geophys.*, *55*, 509–559, doi:10.1002/2016RG000540.
- Turpin, B. J., and J. J. Huntzicker (1995), Identification of secondary organic aerosol episodes and quantitation of primary and secondary organic aerosol concentrations during SCAQS, *Atmos. Environ.*, *29*(23), 3527–3544, doi:10.1016/1352-2310(94)00276-q.
- Twomey, S. (1977), Influence of pollution on shortwave albedo of clouds, *J. Atmos. Sci.*, *34*(7), 1149–1152, doi:10.1175/1520-0469(1977)034<1149:tiopot>2.0.co;2.
- Weinstein-Lloyd, J., and S. E. Schwartz (1991), Low-intensity radiolysis study of free-radical reactions in cloudwater: H_2O_2 production and destruction, *Environ. Sci. Technol.*, *25*, 791–800.
- Wonaschuetz, A., A. Sorooshian, B. Ervens, P. Y. Chuang, G. Feingold, S. M. Murphy, J. de Gouw, C. Warneke, and H. H. Jonsson (2012), Aerosol and gas re-distribution by shallow cumulus clouds: An investigation using airborne measurements, *J. Geophys. Res.*, *117*, D17202, doi:10.1029/2012JD018089.
- Woo, J. L., and V. F. McNeill (2015), Simple GAMMA v1.0—A reduced model of secondary organic aerosol formation in the aqueous aerosol phase (aaSOA), *Geosci. Model Dev.*, *8*(6), 1821–1829, doi:10.5194/gmd-8-1821-2015.
- Yuen, P., D. A. Hegg, and T. V. Larsson (1994), The effects of in-cloud sulfate production on light-scattering properties of continental aerosol, *J. Appl. Meteorol.*, *33*, 848–854.